

Impact of p-GaN thickness on the transport properties of two-dimensional hole gases in a GaN/AlGaN/GaN heterostructure

Pengfei Shao(邵鹏飞), Yifan Cheng (成毅凡), Yu Liu(柳裕), Qi Yao(姚齐), Zanjiang Qiao(乔赞江), Yanghu Peng (彭扬虎), Qin Cai(蔡青), Tao Tao(陶涛), Zili Xie(谢自力), Dunjun Chen(陈敦军), Bin Liu(刘斌), Rong Zhang(张荣), and Ke Wang(王科)

Citation: Chin. Phys. B, 2025, 34 (**11**): 117301. DOI: 10.1088/1674-1056/ae0397
http://cpb.iphy.ac.cn; http://iopscience.iop.org/cpb

What follows is a list of articles you may be interested in

Band alignment of heterojunctions formed by $PtSe_2$ with doped GaN

Zhuoyang Lv(吕卓阳), Guijuan Zhao(赵桂娟), Wanting Wei(魏婉婷), Xiurui Lv(吕秀睿), and Guipeng Liu(刘贵鹏)
Chin. Phys. B, 2025, 34 (**4**): 047304. DOI: 10.1088/1674-1056/adb67b

Protection of isolated and active regions in AlGaN/GaN HEMTs using selective laser annealing

Mingchen Hou(侯明辰), Gang Xie(谢刚), Qing Guo(郭清), and Kuang Sheng(盛况)
Chin. Phys. B, 2021, 30 (**9**): 097302. DOI: 10.1088/1674-1056/abf34c

Analysis of the decrease of two-dimensional electron gas concentration in GaN-based HEMT caused by proton irradiation

Jin-Jin Tang(汤金金), Gui-Peng Liu(刘贵鹏), Jia-Yu Song(宋家毓), Gui-Juan Zhao(赵桂娟), and Jian-Hong Yang(杨建红)
Chin. Phys. B, 2021, 30 (**2**): 027303. DOI: 10.1088/1674-1056/abbbf7

Mechanism of Ti/Al/Ni/Au ohmic contacts to AlGaN/GaN heterostructures via laser annealing

Mingchen Hou(侯明辰), Gang Xie(谢刚), Kuang Sheng(盛况)
Chin. Phys. B, 2019, 28 (**3**): 037302. DOI: 10.1088/1674-1056/28/3/037302

Effect of annealing on performance of PEDOT：PSS/n-GaN Schottky solar cells

Feng Qian (冯倩), Du Kai (杜锴), Li Yu-Kun (李宇坤), Shi Peng (时鹏), Feng Qing (冯庆)
Chin. Phys. B, 2014, 23 (**7**): 077303. DOI: 10.1088/1674-1056/23/7/077303

RAPID COMMUNICATION

Impact of p-GaN thickness on the transport properties of two-dimensional hole gases in a GaN/AlGaN/GaN heterostructure

Pengfei Shao(邵鹏飞)[1], Yifan Cheng (成毅凡)[1], Yu Liu(柳裕)[1], Qi Yao(姚齐)[1], Zanjiang Qiao(乔赞江)[1], Yanghu Peng (彭扬虎)[1], Qin Cai(蔡青)[1], Tao Tao(陶涛)[1], Zili Xie(谢自力)[1], Dunjun Chen(陈敦军)[1], Bin Liu(刘斌)[1], Rong Zhang(张荣)[1,2], and Ke Wang(王科)[1,†]

[1] *Jiangsu Provincial Key Laboratory of Advanced Photonic and Electronic Materials, School of Electronic Science and Engineering, Nanjing University, Nanjing* 210093, *China*

[2] *Department of Physics, OSED, Fujian Provincial Key Laboratory of Semiconductors Materials and Applications, Xiamen University, Xiamen* 361005, *China*

(Received 3 June 2025; revised manuscript received 5 August 2025; accepted manuscript online 5 September 2025)

Polarization-induced two-dimensional hole gases (2DHG) in GaN/AlGaN/GaN heterostructures offer a promising pathway for advancing p-channel transistors. This work investigates the impact of p-GaN thickness on hole distribution and transport through temperature-dependent Hall measurements and TCAD simulations. It is demonstrated that the p-channel is composed of holes both in the p-GaN layer and in the 2DHG at the GaN/AlGaN heterointerface at 300 K, whereas at 77 K, the p-channel conduction is dominated solely by the 2DHG at the GaN/AlGaN heterointerface. The results also reveal the formation of a polarization-induced 2DHG at the GaN/AlGaN interface, exhibiting a high sheet density of 2.2×10^{13} cm^{-2} and a mobility of 16.2 cm$^2\cdot$V$^{-1}\cdot$s^{-1} at 300 K. The 2DHG sheet density remains nearly independent of p-GaN thickness when the p-GaN layer exceeds 30 nm. However, for p-GaN layers thinner than 30 nm, the 2DHG sheet density strongly depends on the p-GaN thickness, which is attributed to the gradual extension of the depletion region toward the GaN/AlGaN interface under the influence of surface trap states.

Keywords: gallium nitride, two-dimensional hole gases, transport property, GaN/AlGaN/GaN heterostructure

PACS: 73.61.Ey

DOI: 10.1088/1674-1056/ae0397 **CSTR:** 32038.14.CPB.ae0397

1. Introduction

Benefiting from the superior properties of gallium nitride (GaN) materials, such as a large band gap, high electric field strength, and high two-dimensional electron gas (2DEG) mobility, GaN-based devices show great potential for applications in data centers,[1–3] electric vehicles, optoelectronics, space electronics, power conversion, 5G communication, and electronics operating in harsh environments.[4–10] However, these advantages have not yet been fully realized in GaN p-channel field-effect transistors (p-FETs). Due to the low mobility and carrier concentration in the p-GaN channel, as well as the high source/drain contact and channel resistances,[10–12] GaN p-FETs generally exhibit a much lower current density than n-channel field-effect transistors (n-FETs),[13–15] resulting in a lag in the development of all-GaN-based complementary metal–oxide–semiconductor (CMOS) technology.

Many approaches have been proposed to enhance the current density of enhancement-mode (E-mode) GaN p-FETs, including double-channel p-heterostructures,[16] O_2 surface treatment,[17] p-InGaN polarization layers,[18] H plasma treatment,[19] and others. In addition, achieving high-performance GaN p-FETs involves inducing a two-dimensional hole gas (2DHG) channel that takes advantage of the large polarization discontinuity in nitride heterostructures such as InGaN/GaN,[20] GaN/AlInGaN,[21] GaN/AlGaN/AlN,[22] and GaN/AlN.[23,24] This approach aims to enhance both hole density and mobility. However, implementing CMOS with these structures is challenging due to incompatibility with GaN n-FET technology. To leverage mature n-FET technology, it is essential to develop GaN p-FETs on the AlGaN/GaN platform, where 2DHG and 2DEG coexist.[25,26]

Up to now, the on-current density of these E-mode p-FETs has typically remained below 10 mA/mm[27–29] because of limitations in the conductivity of the 2DHG channel. One effective approach to improving the on-current density of p-FETs is to form a high-hole-density 2DHG channel on the AlGaN/GaN platform. In this work, we carefully design and grow a GaN/AlGaN/GaN heterostructure, focusing on the effect of p-GaN layer thickness on the transport properties of the 2DHG. We demonstrate an optimal heterostructure with a high hole density in the 2DHG by optimizing the p-GaN thickness. This research will further advance the development of GaN-based p-FETs.

†Corresponding author. E-mail: kewang@nju.edu.cn

© 2025 Chinese Physical Society and IOP Publishing Ltd. All rights, including for text and data mining, AI training, and similar technologies, are reserved.

2. Experimental details

The 2DHG heterostructures based on the GaN/AlGaN/GaN platform were grown using a RIBER Compact 21 plasma-assisted molecular beam epitaxy (PA-MBE) system on C-doped GaN/sapphire templates. The growth rate was maintained at 2.0 nm/min, controlled by nitrogen plasma generated at an radio frequency (RF) power of 450 W and an N_2 flow rate of 0.7 standard cubic centimeters per minute.[30] The epilayers were grown at a temperature of 890 °C (thermocouple temperature) under slightly metal-rich conditions. After unloading from the MBE chamber, the samples were dipped in an HCl solution at 80 °C to remove excess Ga metal. High-resolution x-ray diffraction (HRXRD) 2θ–ω scans for the (002) reflection and reciprocal space maps (RSMs) for the (105) reflection were performed using a Bruker D8 Discovery system to determine the Al composition and strain state of the AlGaN buffer layers. The surface morphology of the samples was characterized using atomic force microscopy (AFM). Ohmic contacts were fabricated by depositing Ni/Au (20 nm/20 nm) at the four corners of the sample in a van der Pauw configuration, followed by rapid thermal annealing at 500 °C for 10 min under an oxygen atmosphere. Temperature-dependent Hall-effect measurements were conducted over the range of 300 K to 77 K using a Lake Shore Cryotronics Hall-effect measurement system with an applied magnetic field of 0.5 T.

3. Results and discussion

The schematic of the epilayer structure features p-GaN layers with varying thicknesses of 60 nm (sample A), 40 nm (sample B), and 20 nm (sample C), as shown in Fig. 1(a). The structure consists of a 300 nm unintentionally doped GaN (uid-GaN) 2DEG channel, a 15 nm AlGaN barrier layer with an Al composition of 0.35, a 10 nm uid-GaN 2DHG channel, and a p-GaN layer with an Mg concentration of 1×10^{19} cm^{-3}. Additionally, a 250 nm p-GaN layer with an Mg concentration of 1×10^{19} cm^{-3} was grown on the C-doped GaN/sapphire templates as a control sample (sample D). The structural parameters and extracted data for all samples are summarized in Table 1. The corresponding schematic energy band diagram is shown in Fig. 1(b). The bottom AlGaN/GaN interface contains positive polarization charges that induce a 2DEG, while a polarization-induced 2DHG forms at the GaN/AlGaN interface due to these positive polarization charges.

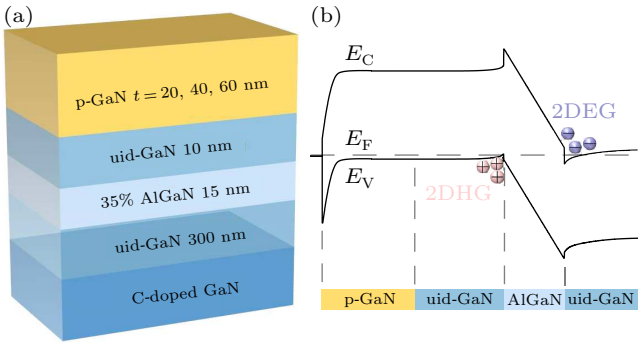


Fig. 1. (a) Schematic of the epilayer structure of p-GaN/uid-GaN/AlGaN/GaN double heterostructures with varying p-GaN thicknesses of 20 nm, 40 nm, and 60 nm, respectively. (b) Schematic of the energy band diagram. The polarization-induced 2DHG forms at the GaN/AlGaN interface. The positive polarization charge at the AlGaN/GaN interface induces a 2DEG.

Figure 2(a) shows the HRXRD 2θ–ω scans of the three samples, measured using a Bruker D8 system with a triple-axis detector along the (002) direction. The diffraction peaks of GaN and AlN from the C-doped GaN/sapphire sample are observed at 34.56° and 36.05°, respectively. The AlGaN peak appears between those of GaN and AlN, exhibiting a broad feature due to the thin 15 nm AlGaN layer. The PendellÖsung fringes observed in the alloyed AlGaN epilayers of all samples indicate a sharp interface between AlGaN and GaN.[15] The light-colored curve in Fig. 2(a) represents the theoretical diffraction pattern simulated using X'Pert Epitaxy. The good agreement between the measured and simulated spectra confirms precise control over the AlGaN thickness and composition. The AlGaN layer, with a thickness of approximately 15 nm, has Al compositions of 0.35, 0.36, and 0.36 for samples A, B, and C, respectively. To analyze the strain state of the AlGaN grown on the thick GaN layer, reciprocal space mapping (RSM) around the asymmetric (105) reflection was performed. Figure 2(b) shows the RSM pattern for sample A. The AlGaN and GaN exhibit the same q_x value, confirming that the AlGaN layer is fully strained to the underlying GaN layer.

Table 1. Overview of structural details of all samples in this work. Temperature dependent sheet hole density, $p_s^{300\ K}$ and $p_s^{77\ K}$, measured by the Hall effect at 300 K and 77 K. 2DHG density at 300 K ($p_{2DHG}^{300\ K}$) has been extracted by excluding the influence of p-GaN layers.

Samples	p-GaN (nm)	AlGaN (nm)	Mg Con. (cm^{-3})	Al com. (x)	R_{SH} (300 K) (kΩ/□)	$p_s^{77\ K}$ (cm^{-2})	$p_s^{300\ K}$ (300 K) (cm^{-2})	$p_{2DHG}^{300\ K}$ (300 K) (cm^{-2})
A	60	15	1×10^{19}	0.35	18.4	1.3×10^{13}	2.3×10^{13}	2.1×10^{13}
B	40	15	1×10^{19}	0.36	15.5	1.3×10^{13}	2.2×10^{13}	2.1×10^{13}
C	20	15	1×10^{19}	0.36	0.49	-7.6×10^{12}	-1.0×10^{13}	–
D	250	–	1×10^{19}	–	96.1	–	1.1×10^{13}	–

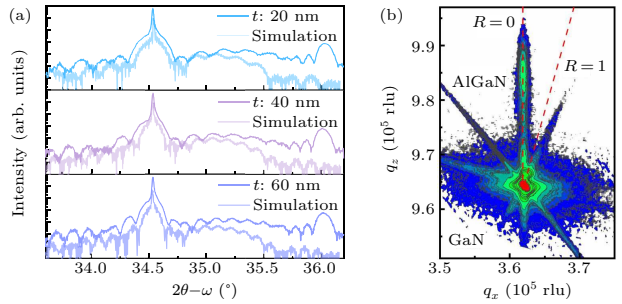


Fig. 2. (a) HRXRD 2θ–ω scans of GaN/AlGaN/GaN structures with varying p-GaN thicknesses of 60 nm (sample A), 40 nm (sample B), and 20 nm (sample C), respectively. (b) Reciprocal space mapping around the asymmetric (105) diffraction for sample A.

The surface morphology of the epilayers was measured using AFM. All samples exhibit atomically flat surfaces with a clear step-flow morphology, and the measured root-mean-square (RMS) roughness is approximately 0.2 nm over an area of 2×2 μm^2, as shown in Fig. 3.

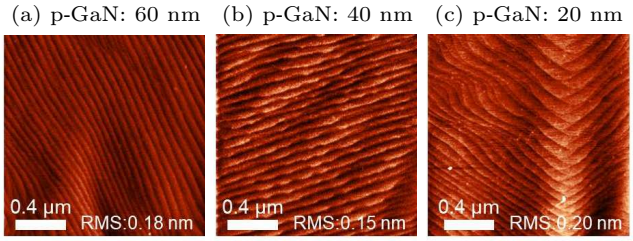


Fig. 3. AFM images of the as-grown surfaces of (a) sample A, (b) sample B, and (c) sample C with a size of 2×2 μm^2.

Temperature-dependent carrier properties of samples A–D were characterized using van der Pauw Hall-effect measurements, as shown in Figs. 4(a)–4(d). For sample D (p-GaN), the hole sheet density exhibits an exponential decrease with decreasing temperature, owing to the partial freeze-out of Mg acceptors at lower temperatures.[31] The activation energy (E_A) of the Mg acceptor was extracted to be approximately 168 meV. Correspondingly, the sheet resistance of sample D increases sharply from 96 kΩ/□ at 300 K to 6400 kΩ/□ at 180 K. In contrast, the hole sheet density and resistance of the other samples show only weak temperature dependence, which directly evidences the existence of polarization-induced 2DHG at the GaN/AlGaN heterointerface.[23] Specifically, in samples A and B, the hole sheet density slightly decreases as the temperature is lowered from 300 K to 180 K, and then remains nearly constant at $\sim 1.3 \times 10^{13}$ cm^{-2} in the low-temperature range of 180–77 K. As reported previously, the measured hole density comprises contributions from both the p-GaN channel and the 2DHG channel at the p-GaN/GaN/AlGaN interface, leading to a mixed temperature-dependent behavior. When the temperature drops to around 180 K in sample A, the hole density decreases from 2.3×10^{13} cm^{-2} to 1.5×10^{13} cm^{-2} due to the freeze-out of holes from ionized Mg acceptors. At lower temperatures, the remaining carriers are primarily attributed to the polarization-induced 2DHG.

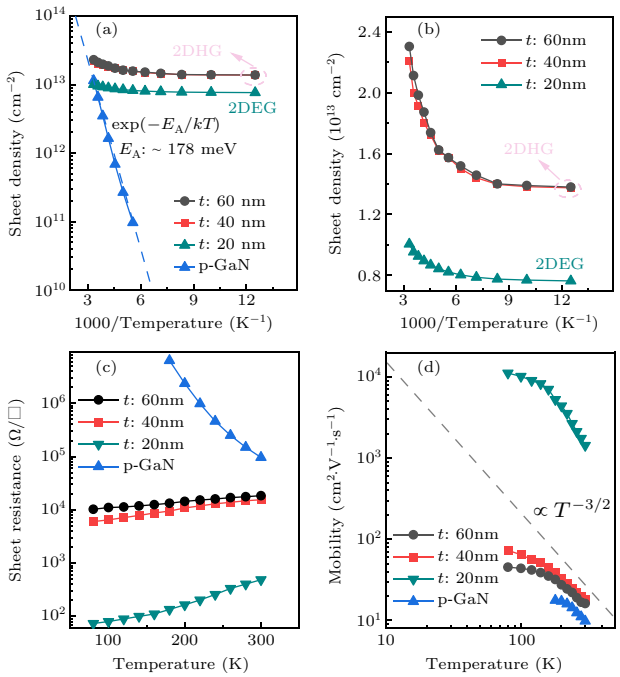


Fig. 4. Logarithmic scale (a) and linear scale (b) of sheet hole density, (c) sheet resistance, and (d) mobility as a function of temperature for samples A, B, and D (control sample).

The temperature dependence of the sheet resistance for all samples is presented in Fig. 4(c). As the temperature decreases from 300 K to 77 K, the 2DHG exhibits metallic-like behavior,[21,22] as evidenced by the notable decrease in sheet resistance of sample A from 18.4 kΩ/□ to 10.2 kΩ/□. In contrast, the sheet resistance of p-GaN increases significantly at low temperatures — a distinguishing feature between 2DHG and p-GaN conduction. The observed reduction in sheet resistance for samples A and B is mainly attributed to enhanced hole mobility at lower temperatures.

Figure 4(d) illustrates the temperature dependence of 2DHG mobility as the temperature decreases from 300 K to 77 K. The mobilities of samples A and B initially follow the $T^{-3/2}$ dashed-line dependence above 180 K. However, they deviate from this trend below 180 K. In the temperature range of 180–300 K, phonon scattering is the dominant mechanism limiting the hole mobility.[32–34] At lower temperatures, the mobility is primarily constrained by interface roughness, alloy disorder, and dislocation scattering. Notably, the mobility at 77 K decreases significantly with increasing p-GaN thickness. This reduction may be attributed to the diffusion of Mg impurities into the 2DHG channel, which enhances impurity scattering.

To elucidate the mechanism of 2DHG formation, the 2DHG sheet densities of the samples with varying p-GaN thicknesses were compared, as shown in Figs. 4(a) and 4(b). Samples A and B exhibit consistent 2DHG sheet densities (p_{2DHG}) in the range of approximately 1.3–1.6×10^{13} cm^{-2} below 180 K, regardless of p-GaN thickness. However, above 180 K, the hole sheet density increases with p-GaN thickness at a fixed Mg concentration of 1×10^{19} cm^{-3}.

A parallel conduction model was proposed to clarify the Hall-effect results

$$p_{\text{total}}(T) = p_{\text{2DHG}}(T) + p_{\text{Mg}}(T), \tag{1}$$

$$p_{\text{Mg}}(T) = t \times [p]_{\text{Mg}}(T), \tag{2}$$

$$[p]_{\text{Mg}}(T) = \frac{(N_{\text{A}}^{\text{i}} - N_{\text{D}}^{\text{i}})N_{\text{V}}}{4N_{\text{D}}^{\text{i}}} \exp\left(-\frac{E_{\text{A}}}{kT}\right), \tag{3}$$

where p_{total} is the measured total hole sheet density, p_{2DHG} is the 2DHG sheet density, and p_{Mg} is the hole sheet density contributed by the p-GaN layer. The term $[p]_{\text{Mg}}$ represents the hole concentration in p-GaN, which can be calculated using Eq. (3) with an activation energy of $E_{\text{A}} = 168$ meV. Here, t is the thickness of the p-GaN layer, N_{A}^{i} is the Mg acceptor concentration, and N_{D}^{i} is the compensating donor concentration (approximately 7×10^{17} cm^{-3} for p-GaN). N_{V} is the effective density of states of the GaN valence band, with an effective hole mass $m_{\text{h}}^{*} = 1.6m_0$, k is the Boltzmann constant, and T is the temperature.

The calculated hole sheet densities for 40 nm and 60 nm p-GaN layers are 1.6×10^{12} cm^{-2} and 2.4×10^{12} cm^{-2}, respectively, consistent with typical values for p-GaN of similar doping levels. It is noteworthy that the hole sheet density of sample A (60 nm p-GaN) is about 1.0×10^{12} cm^{-2} higher than that of sample B (40 nm p-GaN) at 300 K, as shown in Fig. 4(b). Therefore, the increase in hole sheet density with thicker p-GaN is attributed to the thermal activation of Mg acceptors in the p-GaN layer.

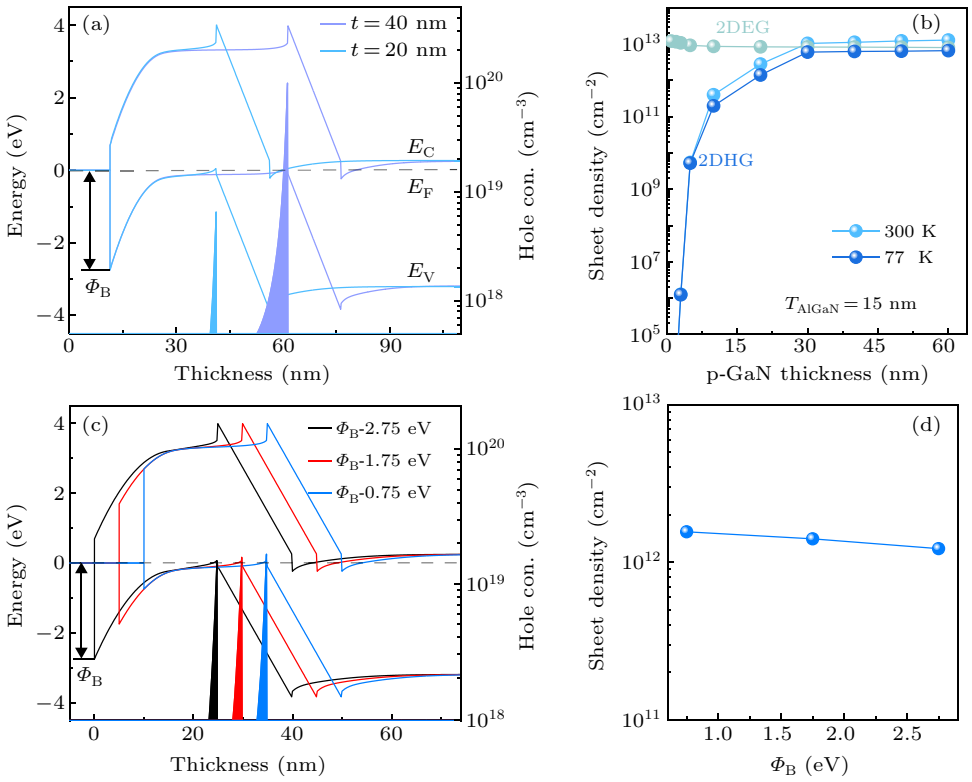


Fig. 5. (a) Band diagrams and the spatial hole distributions of GaN/AlGaN/GaN double heterostructures, and (b) simulated results of 2DHG and 2DEG sheet densities for different p-GaN thicknesses. (c) Band diagrams and the spatial hole distributions of GaN/AlGaN/GaN double heterostructures, and (d) simulated results of 2DHG sheet density for various gate/p-GaN Schottky barrier heights, with the p-GaN thickness fixed at 15 nm.

Additionally, sample C, which has a 20 nm p-GaN layer, exhibits Hall conductivity with a negative Hall coefficient. This behavior is likely caused by surface trap effects. The energy band diagrams and hole distributions near the GaN/AlGaN interface for different p-GaN thicknesses are shown in Fig. 5(a). A triangular quantum well forms at the interface, confining the 2DHG within a width of about 3 nm. The peak hole density decreases markedly as the p-GaN thickness decreases, from 1×10^{20} cm^{-3} at 40 nm to 1.8×10^{19} cm^{-3} at 20 nm. The 2DHG distribution is primarily determined by the band bending at the GaN/AlGaN heterointerface,[23] which can be further enhanced by increasing the p-GaN thickness beyond a critical value.

Figure 5(b) illustrates the simulated variations in 2DHG and 2DEG densities as a function of p-GaN layer thickness. The results clearly indicate the presence of a critical minimum p-GaN thickness required for the formation of 2DHG at the GaN/AlGaN interface. The 2DHG sheet density decreases significantly with increasing p-GaN thickness and gradually approaches saturation. When the p-GaN thickness is less than 15 nm, the 2DHG sheet density is at least one order of magnitude lower than that of the 2DEG. For p-GaN layers thinner than 30 nm, the 2DHG sheet density decreases rapidly, likely due to surface state effects. At a thickness of approximately

30 nm, the 2DHG and 2DEG sheet densities become comparable. Therefore, a relatively thick p-GaN layer (above 30 nm) is essential to achieve a high 2DHG sheet density.

Figure 5(d) further shows that the hole density at the GaN/AlGaN heterointerface slightly decreases with increasing gate/p-GaN Schottky barrier height.

Previous studies have reported that Fermi-level pinning occurs at the GaN surface due to various surface trap states located approximately 0.5–1.7 eV below the conduction band edge.[35–37] These surface states induce a depletion region near the p-GaN surface, which may extend toward the GaN/AlGaN interface. As the p-GaN layer becomes thinner, the depletion region extends deeper, reducing the 2DHG sheet density. However, when the p-GaN layer (with an Mg concentration of 1×10^{19} cm^{-3}) exceeds 30 nm, the surface trap effect is effectively suppressed. Consequently, the 2DHG sheet density remains at a saturated value for p-GaN thicknesses greater than 30 nm, whereas sample C with a 20 nm p-GaN layer exhibits a negative Hall coefficient.

4. Conclusion

In summary, the hole distribution and transport properties of the 2DHG in the p-GaN/GaN/AlGaN/GaN heterostructure were systematically investigated using temperature-dependent Hall-effect measurements. To suppress surface trap effects and achieve a high 2DHG sheet density of approximately 1.3×10^{13} cm^{-2} at 77 K, the p-GaN thickness must exceed a critical threshold of about 30 nm. The measured hole sheet density at 300 K includes contributions from both the p-GaN layer and the 2DHG channel, whereas at 77 K it is dominated solely by the 2DHG. The 2DHG exhibits a nearly temperature-independent hole sheet density, demonstrating its potential for stable p-FET operation across a wide temperature range.

Acknowledgments

This work was supported by the National Key Research and Development Program of China (Grant No. 2024YFE0205000), the Natural Science Foundation of Jiangsu Province, China (Grant No. BK20243037), the National Natural Science Foundation of China (Grant Nos. 62074077 and 61921005), the Postdoctoral Fellowship Program of CPSF (Grant No. GZC20231098), and the Collaborative Innovation Center of Solid State Lighting and Energy-Saving Electronics.

References

[1] Khan M A, Kuznia J, Hove J V, Pan N and Carter J 1992 *Appl. Phys. Lett.* **60** 3027
[2] Khan M A, Bhattarai A, Kuznia J and Olson D 1993 *Appl. Phys. Lett.* **63** 1214
[3] Ambacher O, Smart J, Shealy J, Weimann N, Chu K, Murphy M, Schaff W, Eastman L, Dimitrov R and Wittmer L 1999 *J. Appl. Phys.* **85** 3222
[4] Mishra U K, Shen L, Kazior T E and Wu Y F 2008 *Proc. IEEE* **96** 287
[5] Mishra U K, Parikh P and Wu Y F 2002 *Proc. IEEE* **90** 1022
[6] Zhang H C, Liang F Z, Song K, Xing C, Wang D H, Yu H B, Huang C, Sun Y, Yang L, Zhao X L, Sun H D and Long S B 2021 *Appl. Phys. Lett.* **118** 242105
[7] Zhang H C, Liang F Z, Yang L, Gao Z X, Liang K, Liu S, Ye Y K, Yu H B, Chen W, Kang Y and Sun H D 2024 *Adv. Mater.* **36** 2405874
[8] Then H W, Radosavljevic M, Koirala P, *et al.* 2022 *IEEE International Electron Devices Meeting* 3511
[9] Jiang X, Li C H, Yang S X, Liang J H, Lai L K, Dong Q Y, Huang W, Liu X Y and Luo W J 2023 *Chin. Phys. B* **32** 037201
[10] Hughes B, Chu R, Lazar J and Boutros K 2015 *IEEE International Electron Devices Meeting* 1671
[11] Hahn H, Reuters B, Pooth A, Noculak A, Kalisch H and Vescan A 2013 *Jpn. J. Appl. Phys.* **52** 128001
[12] Nomoto K, Chaudhuri R, Bader S J, Li L, Hickman A, Huang S, Lee H, Maeda T, Then H W, Radosavljevic M, Fischer P, Molnar A, Hwang J C M, Xing H G and Jena D 2020 *IEEE International Electron Devices Meeting* 163
[13] Raj A, Krishna A, Romanczyk B, Hatui N, Liu W, Keller S and Mishra U K 2023 *IEEE Electron Device Lett.* **44** 9
[14] Chen K J, Wei J, Tang G, Xu H, Zheng Z, Zhang L and Song W 2020 *IEEE International Electron Devices Meeting* 2711
[15] Kinzer D 2020 *IEEE International Electron Devices Meeting* 2751
[16] Niu X R, Hou B, Zhang M, Yang L, Wu M, Zhang X C, Jia F C, Wang C, Ma X H and Hao Y 2023 *Chin. Phys. B* **32** 108101
[17] Zheng Z Y, Song W J, Zhang L, Yang S, Wei J and Chen K J 2020 *IEEE Electron Device Lett.* **41** 26
[18] Yu J J, Wei J, Yang J J, Li T, Yang H, Song Y M, Cui J W, Liu S H, Yang X L, Wang M J and Shen B 2025 *IEEE Electron Device Lett.* **46** 139
[19] Yang C, Fu H Q, Peri P, Fu K, Yang T H, Zhou J G, Montes J, Smith D J and Zhao Y J 2021 *IEEE Electron Device Lett.* **42** 1128
[20] Zhang K, Sumiya M, Liao M, Koide Y and Sang L 2016 *Sci. Rep.* **6** 23683
[21] Reuters B, Hahn H, Pooth A, Hollander B, Breuer U, Heuken M, Kalisch H and Vescan A 2014 *J. Phys. D: Appl. Phys.* **47** 175103
[22] Beckmann C, Wieben J, Thorsten Z, Kirchbrücher A, Ehrler J, Stamm R, Yang Z N, Kalisch H and Vescan A 2022 *J. Phys. D: Appl. Phys.* **55** 435102
[23] Zhang Z X, Encomendero J, Chaudhuri R, Cho Y J, Protasenko V, Nomoto K, Lee K, Toita M, Xing H G and Jena D 2021 *Appl. Phys. Lett.* **119** 162104
[24] Chaudhuri R, Bader S J, Chen Z, Muller D A, Xing H G and Jena D 2019 *Science* **365** 1454
[25] Nakajima A, Liu P C, Ogura M, Makino T, Kakushima K, Nishizawa S, Ohashi H, Yamasaki S and Iwai H 2014 *J. Appl. Phys.* **115** 153707
[26] Shao P F, Fan X, Li S Q, Chen S L, Zhou H, Liu H, Guo H, Xu W Z, Tao T, Xie Z L, Lu H, Wang K, Liu B, Chen D J, Zheng Y D and Zhang R 2023 *Appl. Phys. Lett.* **122** 142102
[27] Su H, Zhang T, Xu S, Tao H, Zhang J and Hao Y 2023 *IEEE Electron Device Lett.* **44** 1939
[28] Zhang Y, Sun Z, Wang W, Liang Y, Cui M, Zhao Y, Wen H and Liu W 2023 *IEEE Trans. Electron Devices* **70** 31
[29] Li T, Zhang M, Yu J, Cui J, Yang J, Wu Y, Yang H, Zhang Y, Yang X, Wang M, Feng S, Shen B and Wei J 2024 *IEEE Trans. Electron Devices* **71** 2361
[30] Li Z H, Shao P F, Shi G J, Wu Y Z, Wang Z P, Li S Q, Zhang D Q, Tao T, Xu Q J, Xie Z L, Ye J D, Chen D J, Liu B, Wang K, Zheng Y D and Zhang R 2020 *Chin. Phys. B* **31** 018102
[31] Ng Y H, Zheng Z Y, Zhang L, Liu R Z, Chen T, Feng S R, Shao Q M and Chen K J 2023 *Appl. Phys. Lett.* **123** 142106
[32] Vurgaftman I and Meyer J R 2003 *J. Appl. Phys.* **94** 3675
[33] Zhong Z Y, Ambacher O, Link A, Holy V, Stangl J, Lechner R T, Roch T and Bauer G 2002 *Appl. Phys. Lett.* **80** 3521
[34] Chaudhuri R, Chen Z, Muller D A, Xing H G and Jena D 2021 *Jpn. J. Appl. Phys.* **130** 025703
[35] Hashizume T and Nakasaki R 2002 *Appl. Phys. Lett.* **80** 4564
[36] Köhler K, Wiegert J, Menner H P, Maier M and Kirste L 2008 *J. Appl. Phys.* **103** 023706
[37] Barbet S, Aubry R, Forte-Poisson M A, Jacquet J C, Deresmes D, Mélin T and Théron D 2008 *Appl. Phys. Lett.* **93** 212107